Supporting Information for:

Optimized Efficiency in InP Nanowire Solar Cells with Accurate 1D Analysis

Yang Chen[1], Pyry Kivisaari[1], Mats-Erik Pistol[1] and Nicklas Anttu[1,2]

1. *Division of Solid State Physics and NanoLund, Lund University, Box 118, 22100 Lund, Sweden*
2. *Sol Voltaics AB, Scheelevägen 22, SE-22363 Lund, Sweden*

The use of g_{1D} for photogeneration profile 2

Optical generation with finite element method and scattering matrix method 2

Comparison of 1D and 3D results 3

Carrier concentration and recombination 4

Mobility in doped region 6

The use of g_{1D} for photogeneration profile

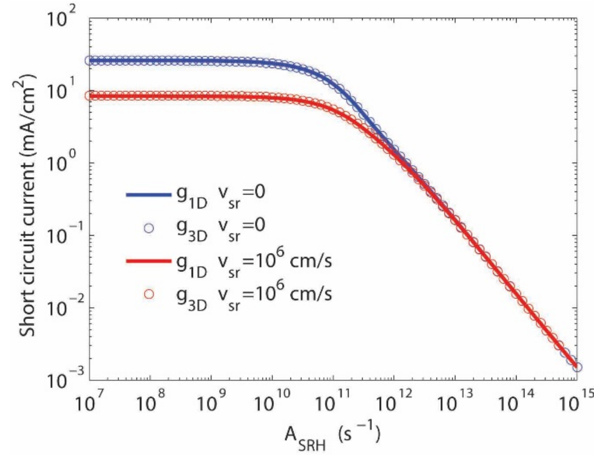

Figure S1. Short-circuit current density for varying A_{bulk} at $v_{\mathrm{sr}} = 0$ and $v_{\mathrm{sr}} = 10^6$ cm/s with g_{1D} and g_{3D} in 3D modeling (the other parameters for the nanowire array are the same as for the standard system in the main text).

Optical generation with finite element method and scattering matrix method

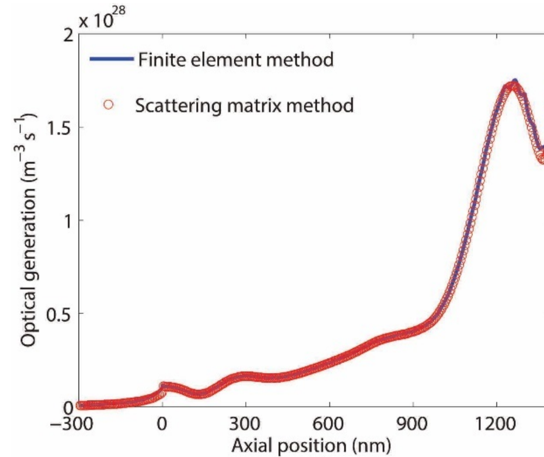

Figure S2. 1D optical generation g_{1D} calculated with scattering matrix method and finite element method. We use the same parameters for the nanowire array as for the standard system in the main text.

In the main text, we calculate the 3D optical generation rate g_{3D} with the finite element method (through Comsol Multiphysics) and transfer it to the 1D generation rate g_{1D} with Eq. (2). Alternatively, we can employ the scattering matrix method [1] to calculate the power flow $F(z,\lambda)$ through the system. From $F(z,\lambda)$, we can calculate g_{1D}(z) [2]. In our experience, a calculation of g_{1D} with $F(z,\lambda)$ from the scattering matrix method can be three orders of magnitude faster than with g_{3D} from the finite element method (see Figure S2 for the g_{1D} calculated with both methods).

Comparison of 1D and 3D results

We show both 3D and 1D modeling results in Figure S3 to demonstrate the validity of Eqs. (7) and (8) for 1D modeling. First, the mobility dependence of the short circuit current is studied as a function of surface recombination velocity. The mobility of electrons and holes is fixed to a constant ratio α compared to the mobility in intrinsic InP. In Figure S3a, results for $\alpha = 0.1$, 1, and 10 are shown from both 3D and 1D modeling. The results from the 1D modeling agree with the results from the 3D modeling, showing the validity for our system of the dependence on α in Eq. (8). In Figure S3b, we show the current-voltage response at surface recombination velocity of 10^5 cm/s to further illustrate the validity of Eq. (7) for varying α. In Figures S3c and S3d, we show results for varying nanowire radius, and find good agreement between 1D and 3D modeling when Eqs. (7) and (8) are used in the 1D modeling for varying r_{NW}.

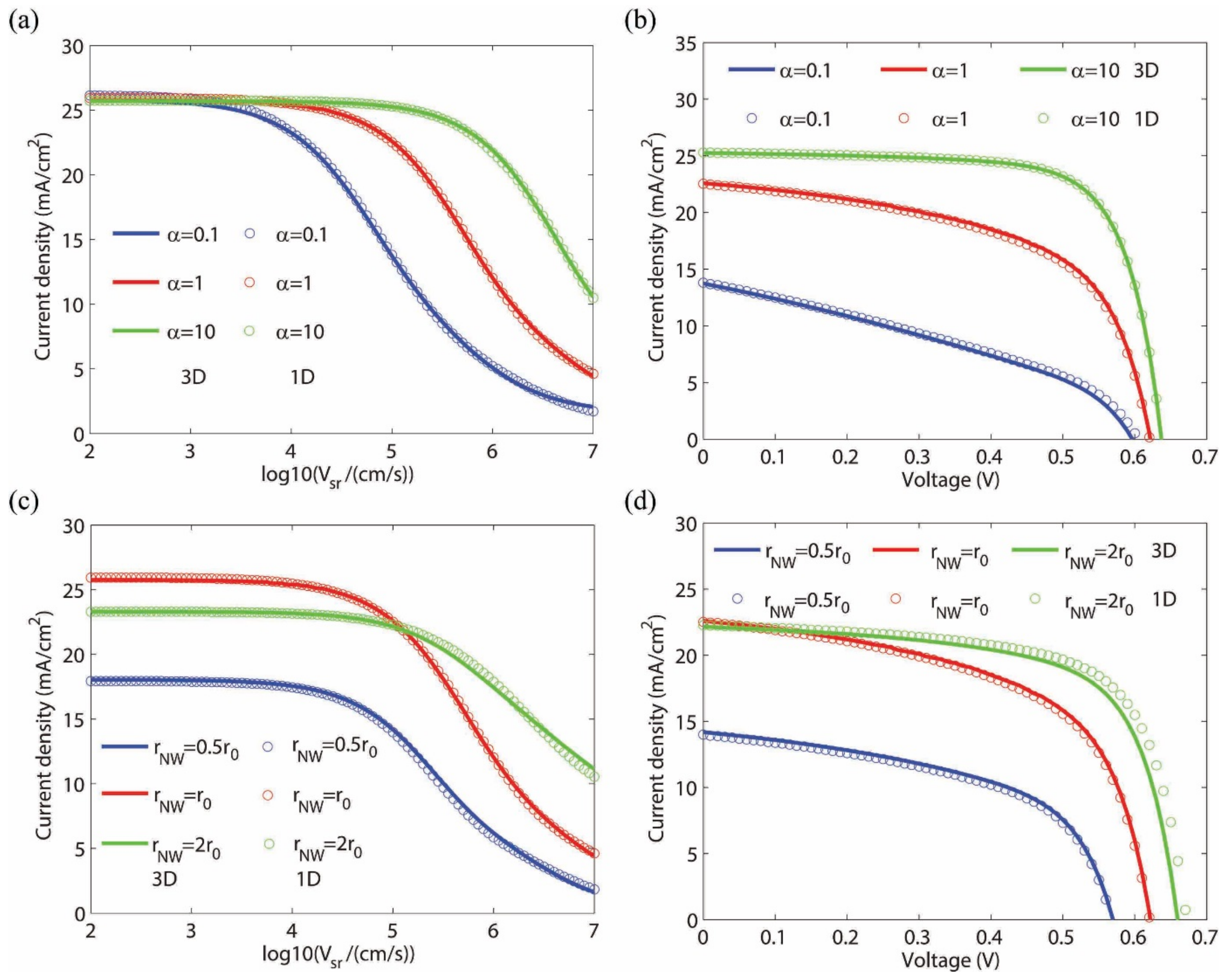

Figure S3. Comparison of 3D and 1D modeling results with A_{eff} from Eqs. (7) and (8) for 1D modeling. (a) Short circuit current for varying surface recombination velocity. (b) Current voltage response for different carrier mobilities $\mu = \alpha\mu_{\mathrm{InP}}$ at a surface recombination velocity of 10^5 cm/s. (c) Short circuit current for varying v_{sr} and (d) current voltage response at fixed $v_{\mathrm{sr}} = 10^5$ cm/s for varying nanowire radius ($r_0 = 90$ nm). Note that in (c) and (d), the pitch P of the nanowire array is scaled to keep the ratio r_{NW}/P constant at the value of 90/330 used in the main text.

Carrier concentration and recombination

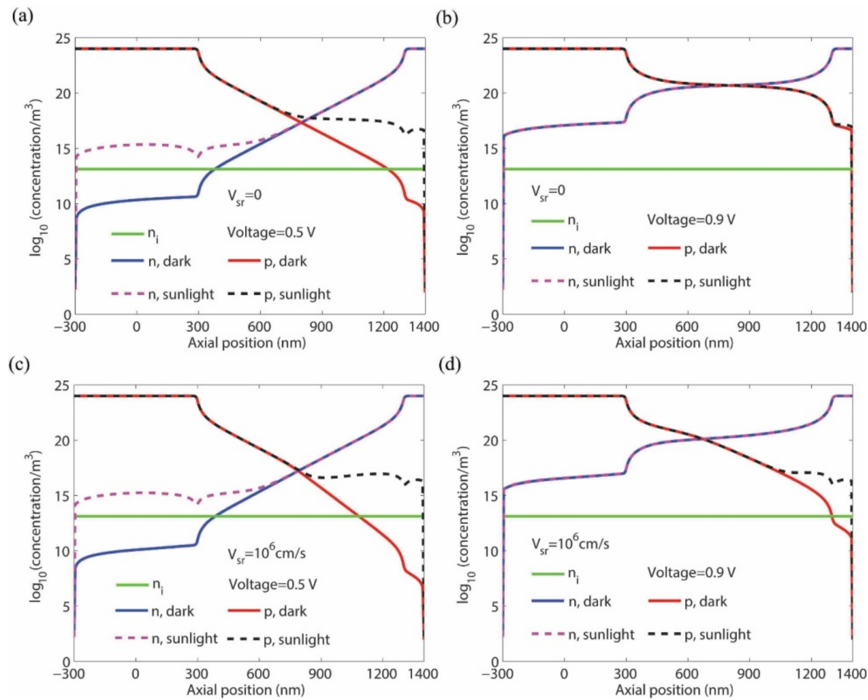

Figure S4. (a)-(b) Carrier concentrations for zero surface recombination velocity at voltage of (a) 0.5 V and (b) 0.9 V, which is the V_{oc} for this $v_{sr} = 0$ as seen in Figure 2c. (c)-(d) Carrier concentration with high surface recombination velocity of 10^6 cm/s at voltage of (c) 0.5 V, which is the V_{oc} for this $v_{sr} = 10^6$ cm/s as seen in Figure 2c, and (d) 0.9 V.

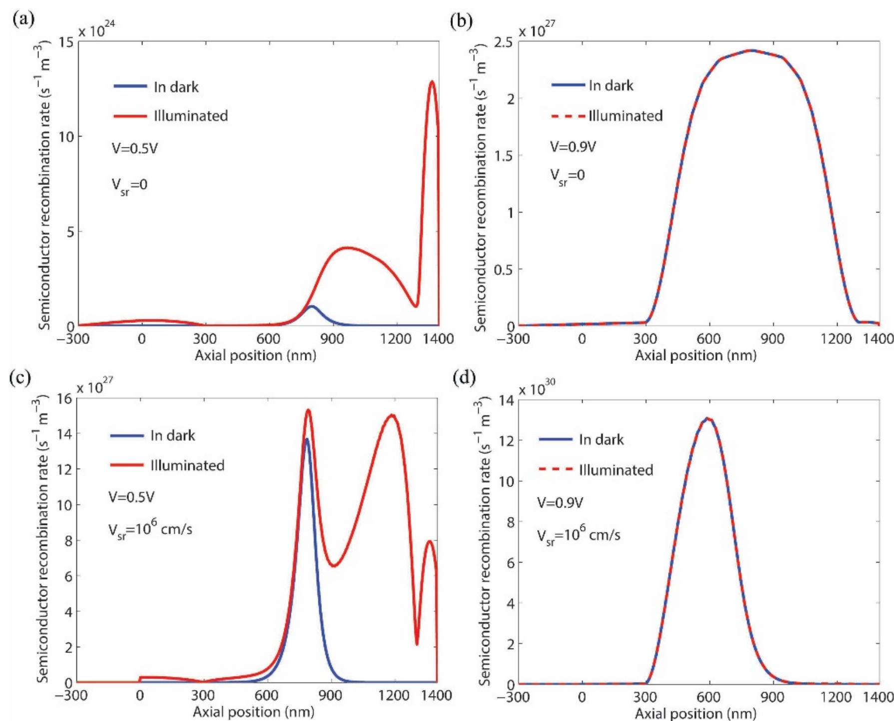

Figure S5. Semiconductor recombination rate, which is the sum non-radiative SRH bulk and surface, radiative, and Auger recombination, with zero surface recombination velocity at voltage of (a) 0.5 V and (b) 0.9 V. Semiconductor recombination rate with high surface recombination velocity of 10^6 cm/s at voltage of (c) 0.5 V and (d) 0.9 V.

To further explain the reason why the superposition principle breaks down in Figure 1b, carrier recombination, which depends on the carrier concentration, can be studied. The recombination rate in the semiconductor is given in the 1D modeling by [3]:

$$R = R_A + R_{rad} + R_{Aug} = (\frac{A_{bulk}+A_{eff}}{n+p+2n_i} + B + C(n+p))(np - n_i^2) \qquad \text{(S1)}$$

where n/p is the electron/hole concentration, A_{eff} is the effective surface recombination coefficient described in Eqs. (6)-(8) in the main text, $A_{\mathrm{bulk}}/B/C$ is the recombination coefficient of bulk SRH/radiative/Auger recombination, and n_{i} is the intrinsic carrier concentration.

In Figure S3, we show the carrier concentration at a lower voltage of 0.5 V and at a higher voltage of 0.9 V for both $v_{\mathrm{sr}} = 0$ and $v_{\mathrm{sr}} = 10^6$ cm/s. At the lower voltage of 0.5 V, for both the high and zero surface recombination velocity, the minority carrier concentration is considerably higher in the illuminated case compared to in the dark case. In contrast, at the higher voltage of 0.9 V, the difference is much smaller. Such a difference in the carrier concentrations at low voltage increases the term (np-n_{i}^2), which increases the recombination in Eq. (S1) by orders of magnitude in the illuminated case as seen in Figure S5a,c.

However, at zero (or low enough) surface recombination velocity at this applied voltage of 0.5 V, the recombination rate is at the order of 10^{23} to 10^{24} $\mathrm{m^{-3}s^{-1}}$ (Figure S5a) which is orders of magnitude lower than the optical generation rate, which is at the level of 10^{27} to 10^{28} $\mathrm{m^{-3}s^{-1}}$ (See Figure S2). Therefore, this additional recombination in the illuminated case is negligible compared to the photogenerated current and hence $J \approx J_{\mathrm{sc}}$, and the superposition principle holds at a low voltage when v_{sr} is low. Note that for this $v_{\mathrm{sr}} = 0$ at $V = 0.9$, which is close to the V_{oc} as seen in Figure 2c, the recombination rate is very similar between the illuminated and dark case (Figure S5b) and $J = J_{\mathrm{sc}} - J_{\mathrm{dark}}(\mathrm{V})$ holds again. We ascertained that the difference in recombination in the illuminated and dark case was for $v_{\mathrm{sr}} = 0$ very minor, relative to the photogeneration rate, between $V = 0.5$ V and $V = 0.9$ V (not shown), and hence the superposition principle holds in general.

In contrast, at the higher surface recombination velocity of $v_{\mathrm{sr}} = 10^6$ cm/s, the recombination rate is comparable to the optical generation rate at $V = 0.5$ V (compare Figure S3c and Figure S2). Therefore, the additional recombination in the illuminated case has a strong impact on the IV-curve, leading to a clear break down of the superposition principle with $J(V) < J_{\mathrm{sc}} - J_{\mathrm{dark}}(V)$, as seen in Figure 1b. Note that also for this $v_{\mathrm{sr}} = 10^6$ cm/s, the recombination rate between the illuminated and the dark case at $V = 0.9$ V are very similar (Figure S4d), and hence the superposition principle holds. However, at this $V = 0.9$ V, which is well beyond the open-circuit voltage of 0.5 V for $v_{\mathrm{sr}} = 10^6$ cm/s, $J \approx J_{\mathrm{dark}}(V)$ and the superposition principle becomes trivial.

Mobility in doped region

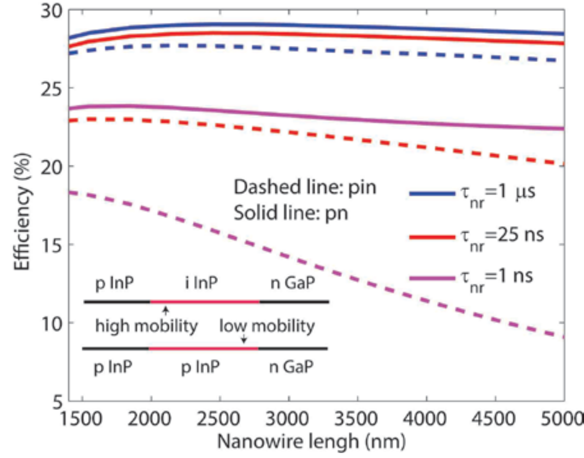

Figure S6. InP nanowire solar cell with either a pn-junction (solid lines) or a pin-junction (dashed lines). Compared to Figure 4 in the main text, here the mobility in the p doped segment (red segment in the schematic in the inset) is reduced. GaP substrate and gradient doping is not shown in the inset figure. The other parameters are the same as in Figure 4 (b) and (c) in main text.

As a doped segment tends to have a lower mobility than an intrinsic segment, we show in Figure S6 the possible effect of such reduced mobility. The relation between the mobility and the doping concentration was approximated by the following equation in p doped InP:

$$\mu_p = \frac{\mu_{p0}}{(1+(\frac{Na}{2\times10^{17}})^{0.5})} \quad \text{(S2)}$$

where μ_{p0}=150 cm^{2}V^{-1}s^{-1} for InP and N_a is the acceptor doping level in unit cm^{-3} [4, 5].

In the doping region, we used p doping level of 10^{18} cm^{-3} in this work and assume that in the intrinsic region, N_a is close to zero. With equation S2, the hole mobility is about 3 times lower in the p doped region than in the intrinsic region. For illustration, we reduce the electron mobility in the p region with the same factor of 1/3. The results are shown in Figure S6 by solid lines. At short carrier lifetime of 1 ns (solid magenta line in Figure S6), this reduced mobility leads to a 1% drop in the highest solar cell efficiency compared to in Figure 4 (c) in the main text. At long carrier lifetime, the highest efficiency drop is smaller than 1%.

References

1. Anttu, N. and H. Xu, *Scattering matrix method for optical excitation of surface plasmons in metal films with periodic arrays of subwavelength holes.* Physical Review B, 2011. **83**(16): p. 165431.
2. Ghahfarokhi, O.M., et al., *Performance of GaAs nanowire array solar cells for varying incidence angles.* IEEE Journal of Photovoltaics, 2016. **6**(6): p. 1502-1508.
3. Chen, Y., et al., *Optimization of the short-circuit current in an InP nanowire array solar cell through opto-electronic modeling.* Nanotechnology, 2016. **27**(43): p. 435404.

4. *http://www.ioffe.ru/SVA/NSM/Semicond/InP/electric.html#Hall.*
5. Wiley, J.D., *Semiconductor and Semimetals, Chapter 2 Mobility of Holes in III-V Compounds.* 1975.